Climatology of Arctic temperature inversions in current and future climates

Cairo J. Ruman, Adam H. Monahan, and Laxmi Sushama

2022

This version of the article has been accepted for publication, after peer review (when applicable) and is subject to Springer Nature's AM terms of use, but is not the Version of Record and does not reflect post-acceptance improvements, or any corrections. The Version of Record is available online at: https://doi.org/10.1007/s00704-022-04147-9

Climatology of Arctic temperature inversions in current and future climates

Caio Jorge Ruman,[a] Adam Hugh Monahan,[b] Laxmi Sushama,[a]

[a] *Department of Civil Engineering and Applied Mechanics, McGill University, Montréal, QC, Canada*

[b] *School of Earth and Ocean Sciences, University of Victoria, Victoria, BC, Canada*

Corresponding author: Caio Jorge Ruman, caio.ruman@mail.mcgill.ca

ABSTRACT

Temperature inversions are a common feature of the Arctic climate, affecting the surface energy budget and planetary boundary layer transports. This study investigates the evolution of large-scale temperature inversions (between 925 hPa and 2m) in the context of a changing climate. To this end, two five-member Regional Climate Model (RCM) ensembles, driven by the Canadian Earth System Model, spanning the 1950–2099 period, corresponding to two greenhouse gas emission scenarios (RCP 4.5 and 8.5), are considered. An ERA-Interim driven simulation for the 1979–2005 period is also considered to assess model performance. A comparison of observed atmospheric soundings with the boundary layer variations in the reanalysis-driven simulation indicates that the model captures the temperature inversion characteristics reasonably well, with some positive biases in the temperature inversion strength and frequency. The transient regional climate change simulations suggest substantial decreases in both temperature inversion strength and frequency in winter in future climate for both emission scenarios. These changes are consistent with the reduced sea ice cover and the associated increase in cloud cover that reduce the surface radiative cooling necessary for the formation of strong temperature inversions. Some increases in the frequency and strength of temperature inversions are projected for summer over the Arctic Ocean, possibly linked with increased poleward moisture transport.

Keywords: temperature inversion, Arctic climate, climate change, regional climate modeling

1. Introduction

Temperature inversions, in which atmospheric temperature increases with height, are a frequent feature of the atmospheric boundary layer in the Arctic. The main temperature inversion formation mechanisms in the Arctic are surface radiative cooling (especially during the polar night), the advection of warm air masses over cooler surfaces, and large-scale subsidence warming in high-pressure situations. Consideration of temperature inversions is important to better understand high-latitude climate change, as they are a crucial feature of the Arctic climate, influencing the surface energy balance and contributing to Arctic amplification of anthropogenic climate change (Serreze and Barry, 2013). Each formation mechanism favors a different type of temperature inversion in the Arctic. Surface radiative cooling can lead to surface-based inversions and are more common in winter months, while large-scale subsidence and advection of warm air tend to form elevated inversions, commonly found in the summer. The temperature inversions can have varied types of structures, from simpler types to multiple inversions layers in the boundary layer, with a mix of surface-based and elevated inversions.

Arctic temperature inversions have been analyzed using data derived from satellites and radiosondes (Liu et al., 2006; Devasthale et al., 2010; Zhang et al., 2021), a combination of model simulations and radiosondes (Zhang et al. 2011), and climate models and reanalyses (Medeiros et al., 2011; Wetzel and Brümmer, 2011). Many studies have used the algorithm described by Kahl (1990) to compute the temperature inversion strength and height, and recently Fochesatto (2015) published a methodology for determining multilayered temperature inversions. Both methods require data from multiple layers in the lower levels of the atmosphere. In contrast, other studies have measured the temperature inversion by differencing temperatures between a selected pressure level above the planetary boundary layer (PBL) and either 1000 hPa or the surface temperature (e.g. Bintanja et al. (2011) and Medeiros et al. (2011)).

In the present study, we focus on the assessment of projected changes to large-scale Arctic temperature inversion characteristics, motivated by their important role in the Arctic climate. We use regional climate model (RCM) simulations for two future emission scenarios and verify the model results using reanalysis, observations from radiosondes, and satellite data. As we are focusing on large scale inversions in an RCM with relatively coarse vertical resolution, multi-layer techniques such as those of Fochesatto (2015) cannot be used and the detailed structure of the temperature inversion structure is not resolved. As such, the present study defines the temperature inversion strength as the temperature difference between the 925 hPa pressure level and the 2m surface temperature. Estimating the temperature inversion strength by the temperature difference between two levels is a crude estimate of the temperature inversion strength, but reasonable when being used to analyze the large-scale structures and the stability of the lower troposphere in climate models which often have a coarse vertical resolution (Medeiros et al. 2011).

Most previous research has focused on winter temperature inversions, as they are more prevalent in that season due to the relatively strong radiative cooling. Summer temperature inversions' frequency and properties are much less dependent on surface net radiation and are largely regulated by the surface melt, poleward intrusion of warm air, and subsidence caused by the presence of polar high (Palo et al. 2017; Zhang et al. 2021). External forcings potentially have a stronger influence on the summer temperature inversion properties than local feedbacks. Most of the Arctic temperature inversion studies in the literature focus on present-day climatologies based on different models and reanalyses (e.g. Zhang & Seidel, 2011; Wang et al, 2020; Chang et al., 2021;). Few studies have investigated future changes in Arctic temperature inversions, with Zhang et al. (2021) focusing on the shallowing of temperature inversion depth and Koenigk et al. (2020) showing that the winter temperature inversion strength is greatly reduced in their work on the Arctic climate change in the 21st century. This study will be one of the first to investigate changes to temperature inversion strength and frequency in future climate projections for the Arctic.

The outline of this paper is as follows. The model, data, and methods used in this research are presented in section 2. Model assessment of temperature inversion characteristics and their projected changes are presented in Section 3. Conclusions are summarized in section 4.

2. Model, Data, and Methods

2.1 Model

The regional climate model used in this study is the Global Environment Multiscale (GEM) model (Côté et al. 1998) in a limited area mode (Teufel and Sushama, 2019). It has a non-hydrostatic dynamical core and uses the Arakawa C grid staggering in the horizontal and vertical coordinate based on hydrostatic pressure (Yeh et al. 2002). The numerical scheme is a two-time-level, semi-Lagrangian, implicit scheme. The GEM physics package includes: deep convection following Kain and Fritsch (1990), shallow convection based on a transient version of the Kuo (1965) scheme (Bélair et al. 2005), large-scale condensation (Sundqvist et al. 1989), correlated K solar and terrestrial radiation (Li and Barker, 2005), subgrid-scale orographic gravity wave drag (McFarlane 1987), low-level orographic blocking (Zadra et al. 2003), and turbulent kinetic energy closure to estimate turbulent fluxes (Benoit et al., 1989; Delage, 1997; Delage and Girard, 1992). Lakes, both resolved and subgrid-scale, are represented by the Flake model (Mironov et al. 2010). The land surface scheme in GEM is the Canadian Land Surface Scheme (CLASS) (Verseghy, 2009), which allows a flexible soil layer configuration. CLASS includes prognostic equations for energy and water conservation for the soil layers and a thermally and hydrologically distinct snowpack where applicable.

This study uses two GEM ensembles of 5 members each, which are driven by five different members of a second-generation Canadian Earth System Model (CanESM2) initial condition ensemble, spanning the 1950–2099 period. The model experimental domain is displayed in Fig. **1**. The two ensembles correspond to RCP 4.5 and 8.5 scenarios (van Vuuren et al. 2011). The RCP 4.5 has an aggressive but not implausible mitigation scenario (IPCC 2013) in which at the end of the current century the global temperature rises slightly above the +2 °C global mitigation aim. The RCP 8.5 is a high-end scenario, where no mitigation is done due to the absence of policies on climate change, and greenhouse gas emissions continue to grow due to high energy demands (Riahi et al. 2011). CanESM2 (Chylek et al. 2011) consists of the physical coupled atmosphere-ocean model, the Fourth Generation Coupled Global Climate Model (CanCM4), coupled to a terrestrial carbon model (CTEM) and an ocean carbon model (CMOC). The simulations driven by CanESM2 will be referred to as GEM-CAN hereafter. An additional ERA-Interim (Berrisford et al. 2009; Dee et al. 2011) driven simulation, named GEM-ERA, for the 1979–2015 period is used to assess the model's ability to simulate the temperature inversion characteristics based on available observations as discussed below. All model results presented below are ensemble means across the five ensemble members for each RCP.

2.2 Observation Datasets and Reanalysis Products

The monthly averaged daily temperature dataset of the University of East Anglia Climate Research Unit (CRU, version TS 4.03; Harris et al., 2014) is used to assess model simulated temperatures over land. This dataset is available at 0.5° resolution and covers the global land surface. The Aqua/AIRS L3 Daily Standard Physical Retrieval V7 dataset - AIRX3STD (AIRS project 2019), with 1° horizontal resolution is used to assess the simulated temperature and temperature inversion characteristics over the Arctic Ocean. The AIRS satellite has a sun-synchronous orbit, passing over the same location each day at 1h30 AM/PM local time (respectively the ascending and descending passes). Devasthale et al. (2010) showed that over the Arctic region, the difference in the temperature inversion strength is generally minimal between those two passes, so in this analysis, both passes were combined. The ERA-Interim reanalysis (Berrisford et al. 2009; Dee et al. 2011) is also used for the assessment of the 2m temperature. ERA-Interim is a global atmospheric reanalysis produced by the European Centre for Medium-Range Weather Forecasts (ECMWF) and covers the years from 1979 to the present time.

Observational radiosonde data from the Integrated Global Radiosonde Archive (IGRA) dataset (Durre et al. 2006) are used to assess model simulated temperature inversion strength and frequency. The radiosonde data are available twice daily (00UTC and 12 UTC) at more than 1500 locations around the globe, 153 of which are located inside the study domain. The IGRA data pass quality assurance algorithms, checking for format problems, climatological outliers, physically improbable values, and temporal and spatial discrepancies in temperature. Only stations with at least 80% of data during the 2003–2015 period are used for model assessment.

2.3 Methods

Before studying projected changes to temperature inversion strength and frequency, the ability of the model to simulate these is assessed by comparing GEM-ERA with available observations and reanalyses datasets. Reanalyses and satellite data provide a comprehensive set of data-informed climate variables for such comparisons. Based on the study of three different reanalyses, Lindsay et al. (2014) identify ERA-Interim as the most consistent with independent measurements in the Arctic. ERA5 was not used in the GEM-ERA simulation as it was released after the model simulation was completed. The simulated 2m temperatures are assessed using CRU data, AIRS, and ERA-Interim reanalysis, while the temperature inversion strength and frequency are compared with atmospheric soundings available from the IGRA database and AIRS temperature profiles. The temperature inversion strength is estimated as the temperature difference between the 925 hPa level and the 2m temperature. Temperature inversion frequency is calculated as the ratio of the number of temperature inversion occurrences to the total length of the data record over the period of interest.

The AIRS satellite data is composed of satellite swaths, which have spatial and temporal sampling differences that can affect comparisons with climate models (Tian et al. 2013). To lessen this temporal and spatial bias, when assessing model data against the AIRS dataset, the model output was resampled hourly, and data were extracted from the model reproducing the satellite swaths on the model domain so that the spatial and temporal sampling of the model data is similar to that of the AIRS data.

Hearty et al. (2014) noted that the AIRS data sometimes report nonphysical temperatures near the surface over land, most notably near steep topography. For this reason, comparisons using the AIRS are only made over the oceans. Chang et al. (2018) found that the temperature inversion strength over the ocean is insensitive to cloud fraction variations, making it a good choice for model assessment. Over continental regions, the CRU dataset and the soundings were used instead. Plots using the AIRS data over the land can be found in the supplementary material (Figure S1).

Projected changes to the temperature inversion characteristics and 2m temperature for RCP4.5 and 8.5 scenarios are investigated by considering spatial distributions of 30-year averages of two future periods, mid-century (2040-2069) and late-century (2070-2099), and their differences with the current period of GEM-CAN simulations.

The statistical significance of the comparison between the model and observation datasets, and between the historical and transient period is assessed with the two-sample t-test, with the null hypothesis (H_0) given as $\mu 2 = \mu 1$ and the alternative hypothesis (H_1) given as $\mu 2 \neq \mu 1$, where µ1 and µ2 are the observations and the model data, or the historical and projected data in the climate projection analysis. We test the null hypothesis at the 95% significance level.

3. Results

This section is divided into two parts: 1) model assessment and climatology of the temperature inversions from model and observations and 2) future projections of temperature inversion characteristics. All results from the GEM-CAN simulations presented in this section are based on averages across the five-member ensemble.

3.1 Climatology of the Temperature Inversions: Model and Observations

Comparisons of model-simulated 2m temperatures with CRU (land), AIRS (ocean), and ERA-Interim for winter (DJF) and summer (JJA) are shown in Fig. 2. Comparison with CRU data indicates cold biases between -1 and -6 °C over Europe and West Asia for DJF, while warm biases are noted over the northeastern parts of Eurasia. A cold bias is also present over Northeastern North America (NA) and a warm bias over the Western and Northwestern NA. The pattern and values of the bias over North America are similar to those found by Šeparović et al. (2013) when analyzing a GEM simulation over the NA domain. The strong positive bias relative to the CRU temperatures over Northeast Asia and the negative bias over Greenland should be interpreted with caution due to the sparse network of observations over the Arctic region; the bias is not as strong when comparing the model to the ERA-Interim reanalysis, and it is present when comparing the ERA-Interim with the CRU dataset. We can see that differences between the observational datasets can be as large as or larger than those between the model simulation and observations. Over the ocean, GEM-ERA has a similar spatial bias for both AIRS and ERA-Interim, with a negative bias over the central Arctic of -1 to -2 °C (ERA-Interim) and of -2 to -3 °C (AIRS) and positive bias of 1 to 3 °C over the coastal region of Siberia and Alaska. For winter, the cold biases over the Rockies and Greenland are presumed to be related to the representation of topography in the model. Batrak and Müller (2019) suggests that the warm biases in reanalysis and models are due the missing representation of snow layer on top of the sea-ice. For the summer months, the model shows a persistent cold bias of -1 to -6 °C compared to both CRU and ERA-Interim. This cold bias is most prominent in East-Central Asia and the eastern Canadian Arctic. The cold bias in summer over Arctic Canada and mountain regions is presumed to be related to snow on the ground. Over the Arctic Ocean, GEM-ERA shows a negative bias of -1 to -2 °C when compared with AIRS and ERA-Interim. From the differences of the datasets in figure 2, we found that they are significant for most of the domain. These biases notwithstanding, visual inspection demonstrates that the means from each dataset are reasonably similar for most of the domain, and the model shows good capacity in simulating the temperature patterns for each season, with spatial variability similar to the biases. As the temperature inversion is strongly coupled with trends in surface temperature (Zhang et al. 2011), knowing the surface temperature bias can lead to a better understanding of the model simulation of the temperature inversions.

The next step in the assessment compares the surface temperature inversion strength and frequency in GEM-ERA with those of the sounding data over land and with those of the AIRS dataset over the ocean, again for both winter and summer. The spatial plots in Fig. **3** show the simulated temperature inversion strength and its frequency and the difference between model values and soundings and AIRS for the Pan-Arctic domain for the 2003–2015 period, with the radiosonde data represented by the filled circles.

Radiative cooling of the surface is one of the key processes responsible for surface-based temperature inversion formation, and therefore higher-latitude locations, particularly in Greenland, Alaska, Canada, and Eastern Siberian Russia, experience more frequent and more intense temperature inversions than lower latitude stations in winter, with temperature inversion frequency between 80-100% and temperature inversion strength between 9 and 12°C.

Across the radiosonde data, the highest temperature inversion frequency occurs in the Arctic Canada region and Siberia, with values ranging across the same range of values as the GEM-ERA model, between 80-100%, and the highest temperature inversion strength occurs in the interior of Alaska and Siberia, with values up to 9°C in Alaska and up to 12°C in Siberia. The temperature inversions are stronger and more frequent in winter due to the polar night and the weakening of air-surface thermal coupling by snow cover (e.g. Van de Wiel et al., 2017).

The patterns for the range of the temperature inversion strength and frequency values of North America (NA) are well represented in the simulation, with the largest winter inversion strength biases of 4°C occurring at a few coastal locations (three on the Arctic Ocean and one on west Greenland). Summer temperature inversion strength bias has a pattern of negative values ranging from -0.5 °C to -2 °C on the west NA and positive bias from 0.5°C to 2°C Nunavut, Quebec, and Greenland regions. Temperature inversion frequency has small differences, up to ±20% in both seasons, with a few outliers on coastal Greenland and the west NA Rockies region. The continental Eurasian patterns also show good agreement for both temperature inversion characteristics. The winter temperature inversion strength shows a positive bias of up to 3 °C in the European region and negative bias up to -4 °C in Siberia. Eurasian summer values do not show a defined pattern, with values ranging from -1.5 °C to 2 °C. Over the Arctic Ocean in winter, the GEM-ERA simulation has stronger and more frequent temperature inversions, limited to the region north of NA and the Baffin Bay. Summer produces a small positive bias of up to 1 °C for the temperature inversion strength and up to 20% for the temperature inversion frequency over the Arctic Ocean. The model overrepresents the winter and summer frequency of the temperature inversion in the center of the Arctic Ocean, showing up to 50% more inversions in winter and 30% more inversions in the summer.

Table 1 shows the radiosonde values and standard deviation with corresponding values from the GEM-ERA simulation for summer and winter at eight locations above latitude 60°

selected as the two best and worst results for each positive and negative winter bias of the temperature inversion strength. Results show good agreement between radiosondes and model values, as all model values are within the soundings' one standard deviation range. Overall, the spatial patterns of the temperature inversion strength and frequency from the GEM model are broadly in agreement with the results obtained from the radiosondes and AIRS for both seasons considered, with the largest differences occurring at a few stations in mountainous regions or the Greenland region. The results from the model display patterns and magnitudes that are broadly in accordance with the soundings for the Arctic region, for both seasons.

When comparing the winter temperature inversion strength and frequency in GEM-ERA with those in GEM-CAN (Fig. 4), the main differences are over regions where the sea-ice concentration differs in the two simulations (not shown). This difference between the GEM-ERA and GEM-CAN simulations illustrates the strong relationship between sea ice and temperature inversion in higher latitudes. Pavelsky et al. (2011) showed that sea ice is the principal driver of spatial variability in inversion strength in the Arctic Ocean. Besides the difference in regions where the sea-ice differs between simulations, the similarity of the two simulations demonstrates that driving by the GEM model does not increase the biases of simulated temperature inversions.

3.2 Climate Projections

Fig. **5** and 6 show the winter season current climate (period 1976-2005) and projected changes of temperature inversion strength and frequency in the GEM-CAN simulation for the 2040–2069 and 2070–2099 future periods with respect to the 1976–2005 current reference period. Projections for RCP 8.5 indicate that winter season inversions will become weaker and less frequent, with the greatest change over the Arctic Ocean, where the temperature inversion strength is reduced by up to 5°C and 7 °C by the mid and late century, respectively. Over much of the Arctic Ocean, the temperature inversion frequency ranges from 60% to 100% lower for the 2070–2099 period than at present, with reductions of up to 100% in the ice-free regions (Figure S2, supplementary material), meaning that regions without sea-ice loses the main contributor for temperature inversion formation in winter. Mid-century projected changes are milder, with most of the Arctic Ocean experiencing between 40 and 60% fewer temperature inversions, up to a 100% reduction in the Barents Sea.

The changes in temperature inversion strength and frequency are consistent with the sea-ice loss and increased cloud cover in winter, with the Arctic Ocean becoming increasingly ice-free and cloudy as warming progresses. Wintertime overall cloud cover increases in all regions north of the 70° latitude, for both RCPs (Figure S3, supplementary material). The increased cloud cover is consistent with the enhanced evaporation rates resulting from reduced sea ice cover (Boisvert and Stroeve, 2015). The reduction of sea-ice also increases the surface sensible heat flux, which increases the air temperature and specific humidity in the lower troposphere, leading to an increase of cloud-cover and downward longwave radiation (Kim et al. 2019), creating a vertical feedback mechanism, reducing the sea-ice even further. In the leads and polynyas (Gultepe et al. 2003), and often over open sea areas of the Arctic, the sensible heat flux is often larger than the latent heat flux. Although the GEM model uses a subgrid-scale tiles approach to calculate the heat fluxes, the SST and sea ice fraction are prescribed from the coarse resolution CanESM2, meaning that fine-scale processes associated with these fields are not represented in the model. Increased ice-free areas in the summertime Arctic Ocean absorb more shortwave energy, resulting in increased latent heat flux later in the year (Morrison et al., 2019). The sensible heat flux also increases, which can lead to reduced cloud formation by heating the air and increasing the saturation specific humidity. In the present GEM simulation results, latent heat fluxes dominate these competing processes, resulting in an increase in cloud cover. As the main factor of strong surface-based temperature inversion formation over the

Arctic is radiative cooling, the progressively ice-free ocean, the increase of cloud cover and surface temperature in winter favors a radiative-turbulent near-equilibrium state of the Arctic atmosphere characterized by a cloudy-sky state (e.g. Abraham and Monahan, 2019). The formation of temperature inversions is inhibited, and when temperature inversions occur, they are weaker.

The largest changes to temperature inversion properties are limited to the Arctic Ocean and adjacent water-covered regions. Only the simulations using RCP 8.5 show large spatial changes over continental areas, with less frequent and weaker inversions. The largest changes of temperature inversion strength over land are seen in the Canadian Arctic Archipelago and Northern Siberia for both future periods considered. The changes of temperature inversion frequency over the continents follow broadly the same pattern as that of temperature inversion strength, with changes in the inversion strength decreasing with increasing distance from the ocean. Lawrence et al. (2008) showed that the warming signal due to rapid sea-ice loss can penetrate inland, leading to terrestrial snow cover reduction changing the surface fluxes and planetary boundary layer characteristics (Alexander et al. 2010; Deser et al. 2010) that affect temperature inversion formation.

The RPC 4.5 simulations show similar patterns as RCP 8.5, but with less pronounced changes. For both the temperature inversion strength and frequency, the late 21st century for RCP 4.5 has similar spatial patterns and magnitudes of projected changes as the RCP 8.5 simulation in mid-century. The similarity is consistent with the corresponding RCPs warming signals due to increased CO_2 concentrations. For RCP 4.5, CO_2 stabilizes at ~500 ppm in the late 21st century. This value is reached by RCP 8.5 around mid-century. In the RCP 4.5 simulation, the late 21st century shows a 50% decrease of inversion frequency and inversions up to 5 °C weaker. Mid-century RCP 4.5 has temperature inversions up to 4°C weaker with a 30% reduction in temperature inversion frequency. The regions with complete loss of wintertime sea-ice in the Arctic Ocean region show a 100% reduction of the inversion frequency in both periods.

Summer season values for the current climate and projected changes for the temperature inversion strength and frequency are shown in Fig. **7** and 8, respectively. For both RCPs, projected changes in the summer season show increased temperature inversion strength and frequency over the Arctic Ocean, except for the ocean regions of the Barents Sea and the Norwegian Sea. These regions show temperature inversions up to 1.5 °C weaker, and up to 40% reduction in temperature inversion frequency, in both RCPs. The late 21st century in RCP 8.5 has up to 50% increased inversion frequency over the Arctic Ocean with inversion strength 1.5°C stronger. Except for the Ellesmere Island in the Canadian Arctic Archipelago, Arctic coastal regions show up to 40% fewer inversions, up to 2 °C weaker, with the southern region of the Canadian Arctic Archipelago having the most pronounced changes. The mid-21st century shows similar patterns as the late century, with weaker changes. These relatively large changes in temperature inversion frequency occur in regions in which summer temperature inversions are relatively common (> 40%) in the present climate. The work of Wang et al. (2022) relates positive anomalies of the summer temperature inversions in the Arctic to the sea-ice minimum extremes in September. With the increased frequency of such temperature inversions in the transient projections, the effect on the sea-ice minima is presumed to increase. The increase in frequency and strength of summer temperature inversions can also make Arctic fog events more common, as inversions factor in fog formation (Gilson et al. 2018).

Similar to the winter results, RCP 4.5 has the same pattern of changes as the RCP 8.5 for the inversion strength and frequency, but with smaller changes of both properties. The changes for the mid-century and late 21st century is similar, with the late century showing only slightly higher values. This can be explained by the stabilization of the climate in RCP 4.5 late 21st century.

The increase in strength and frequency of temperature inversions in summer is likely related to the increase in moist static energy transport in the Arctic, increasing the frequency of temperature inversion formation by advection of warm air masses over a cooler surface. Hwang et al. (2011) show an increase in poleward moisture transport in climate projections driven by the increased moisture as the climate warms. Tjernström et al. (2019) discuss the increased atmospheric water content in the Arctic due to the increased intrusion of warmer air masses, also causing strong surface temperature inversions due to subsidence in the summer months. They hypothesize that as the warm air mass is advected oved the melting sea-ice, it triggers the formation of a sharp surface temperature inversion and fog. As the surface is cold, even low humidity in the advected air results in supersaturation. As mechanical surface mixing and cloud-top buoyant mixing act on this system, the Arctic boundary layer gradually becomes more well mixed. The fog and the well-mixed layer deepen, the cloud lifts from the surface and the Arctic boundary layer transforms into a persistent well-mixed cloud-capped boundary layer.

The results discussed above show the changes in temperature inversion characteristics for summer and winter. In winter, the main mechanism of formation is surface long-wave radiation cooling. Reduction in sea ice cover not only results in the loss of a cold surface but allows for increased moisture flux (Serreze et al., 2009; Screen and Simmonds, 2010a; Screen and Simmonds, 2010b;). The increased wintertime cloud cover reduces the surface longwave cooling rate, greatly diminishing the temperature inversion formation by radiative cooling. For summer, subsidence and the transport of southern air masses likely drive the formation of temperature inversions.

4. Summary and Conclusions

In this study, climate projections of large-scale Arctic temperature inversion characteristics were investigated using an ensemble of the GEM climate model simulations for RCPs 4.5 and 8.5. This study includes the assessment of the model performance and characterization of the spatial distribution of the temperature inversion strength and frequency in summer and winter focusing on the large-scale structure of the temperature inversions, as the model cannot capture the fine-scale characteristics of the lower atmosphere.

The model slightly overestimates the temperature inversion strength and frequency in the current climate, with some coastal regions reaching 4°C difference in the temperature inversion strength, and up to 20% difference in the temperature frequency, consistent with the fact that numerical models have difficulty in representing the stable boundary layer, particularly in the Arctic (Fernando and Weil, 2010; Holtslag et al., 2013). For both summer and winter, the results from the model show patterns and magnitudes that are in overall accordance with soundings and the AIRS satellite data in the Arctic region. The spatial variability of the Arctic temperature inversions is strongly influenced by the surface type. In winter, ice-free zones in the North Atlantic have a low frequency of temperature inversions, in contrast with the sea ice covered ocean and snow-covered regions where occurrence frequency exceeds 80%. Summer values of the temperature inversion frequency are higher for near-coastal regions (up to 70% frequency), in contrast to the central Arctic (40% frequency). Analyses of the transient climate change simulations indicate that the loss of sea ice and related increase in cloud cover in winter leads to weaker and less frequent temperature inversions. This reduction in the occurrence of very strongly stratified conditions is consistent with the reduction in surface radiative cooling resulting from increased cloudiness. The increase of cloud cover is associated with an increased surface moisture flux during the winter seasons after the mostly ice-free sea absorbed energy in the summer. It is important to note that changes in cloud cover are model-dependent. Some climate models predict increased autumn cloud cover in the central Arctic (Liu et al. 2012;

Vavrus et al. 2012), while other models predict a decrease (Koenigk et al. 2013), which can change the outcome of temperature inversions in a future climate. Therefore, additional studies should be made with different RCMs and driving GCMs on the area, due to variations in spatial patterns from different driving data and climate scenarios. For ocean regions in the summer, there is an increase in temperature inversion frequency and strength at the end of the 21st century, consistent with an increase in poleward moist energy transport.

With the changes in the Arctic atmosphere seen in the future climate, the current predominant clear cold atmospheric state becomes less frequent. Cloudy and warm conditions that inhibit the formation of temperature inversions become more common. For the winter season, the reduction of sea ice and the increased cloud cover prevents the radiative cooling necessary to the formation of strong temperature inversions, and for the summer, the increased poleward moisture transport likely due to increased synoptic-scale warm air advection over the cooler ice-free ocean causes a higher incidence of temperature inversions.

These results provide information about how large-scale temperature inversions are represented in climate models and about the effects of a warming climate in the Arctic planetary boundary layer, as changes in temperature inversion characteristics have important implications for the Arctic climate system. For example, temperature inversions mediate the surface energy balance (Bradley et al. 1992; Medeiros et al. 2011), restrict the vertical exchange of momentum, heat, moisture, and pollutants between PBL and the free atmosphere (Wetzel and Brümmer, 2011) and are an important contributor to Arctic Amplification (Bintanja et al. 2011). In this study, we analyzed Arctic temperature inversions looking at relatively coarse structures of the planetary boundary layer. Future work benefiting higher vertical resolution and better representation of near-surface processes could focus on simulating the changes of the more detailed vertical structure of the atmosphere.

Acknowledgments.

This work was supported by funding from the Marine Environmental Observation, Prediction, and Response (MEOPAR) and Polar Knowledge Canada (POLAR). CJR acknowledges the support of the McGill Engineering Doctoral Awards (MEDA) program. AHM acknowledges the support of the Natural Sciences and Engineering Research Council of Canada (NSERC), [funding reference number RGPIN-2019-04986]. The GEM simulations in this study were performed on supercomputers managed by Calcul Québec and Compute Canada.

Author Declarations

Funding: This work was supported by funding from the Marine Environmental Observation, Prediction, and Response (MEOPAR)/Polar Knowledge Canada (POLAR) Year of Polar Prediction project "Predicting the Future(s) of Renewable Energy in Canada's Arctic". AHM acknowledges the support of the Natural Sciences and Engineering Research Council of Canada (NSERC), [funding reference number RGPIN-2019-04986].

Conflicts of interest/Competing interests: 'Not applicable'

Availability of data and material: The data presented in this study are available on request from the corresponding author.

Code availability: The code used to generate the plots and to analyze the data can be found at https://github.com/caioruman

Authors' contributions: C. J. Ruman analyzed the data and wrote the manuscript with editorial assistance from L. Sushama and A. Monahan.

Ethics approval: 'Not applicable'

Consent to participate: 'Not applicable'

Consent for publication: 'Not applicable'

REFERENCES

Abraham, C., & Monahan, A. H. (2019). Climatological features of the weakly and very stably stratified nocturnal boundary layers. Part II: Regime occupation and transition statistics and the influence of external drivers. *Journal of the Atmospheric Sciences*, *76*(11), 3485–3504. https://doi.org/10.1175/JAS-D-19-0078.1

AIRS project. (2019). Aqua/AIRS L3 Daily Standard Physical Retrieval (AIRS+AMSU) 1 degree x 1 degree V7.0, Greenbelt, MD, USA, Goddard Earth Sciences Data and Information Services Center (GES DISC). https://doi.org/10.5067/8XB4RU470FJV

Alexander, M. A., Tomas, R., Deser, C., & Lawrence, D. M. (2010). The atmospheric response to projected terrestrial snow changes in the late twenty-first century. *Journal of Climate*, *23*(23), 6430–6437. https://doi.org/10.1175/2010JCLI3899.1

Batrak, Y., & Müller, M. (2019). On the warm bias in atmospheric reanalyses induced by the missing snow over Arctic sea-ice. *Nature Communications*, *10*(1), 1–8. https://doi.org/10.1038/s41467-019-11975-3

Bélair, S., Mailhot, J., Girard, C., & Vaillancourt, P. (2005). Boundary layer and shallow cumulus clouds in a medium-range forecast of a large-scale weather system. *Monthly Weather Review*, *133*(7), 1938–1960. https://doi.org/10.1175/MWR2958.1

Benoit, R., Côté, J., & Mailhot, J. (1989). Inclusion of a TKE Boundary Layer Parameterization in the Canadian Regional Finite-Element Model. *Monthly Weather*

Review, *117*(8), 1726–1750. https://doi.org/10.1175/1520-0493(1989)117<1726:Ioatbl>2.0.Co;2

Berrisford, P., Dee, D., Poli, P., Brugge, R., Fielding, K., Fuentes, M., et al. (2009). *The ERA-Interim Archive Version 2.0*. *ERA report series* (Vol. 1). Shinfield Park, Reading: ECMWF. http://www.ecmwf.int/publications/library/do/references/list/782009

Bintanja, R., Graversen, R. G., & Hazeleger, W. (2011). Arctic winter warming amplified by the thermal inversion and consequent low infrared cooling to space. *Nature Geoscience*, *4*(11), 758–761. https://doi.org/10.1038/ngeo1285

Boisvert, L. N., & Stroeve, J. C. (2015). The Arctic is becoming warmer and wetter as revealed by the Atmospheric Infrared Sounder. *Geophysical Research Letters*, *42*(11), 4439–4446. https://doi.org/10.1002/2015GL063775

Bradley, R. S., Keimig, F. T., & Diaz, H. F. (1992). Climatology of surface-based inversions in the North American Arctic. *Journal of Geophysical Research*, *97*(D14), 15699–15712. https://doi.org/10.1029/92jd01451

Chang, L., Feng, G., Zhang, Y., & He, X. (2018). Effect of cloud fraction on arctic low-level temperature inversions in AIRS observations over both land and ocean. *IEEE Transactions on Geoscience and Remote Sensing*, *56*(4), 2025–2032. https://doi.org/10.1109/TGRS.2017.2772297

Chang, L., Wen, S., Gao, G., Han, Z., Feng, G., & Zhang, Y. (2021). Assessment of temperature and specific humidity inversions and their relationships in three global reanalysis products over the arctic ocean. *Journal of Applied Meteorology and Climatology*, *60*(4), 493–511. https://doi.org/10.1175/JAMC-D-20-0079.1

Chylek, P., Li, J., Dubey, M. K., Wang, M., & Lesins, G. (2011). Observed and model simulated 20th century Arctic temperature variability: Canadian Earth System Model

CanESM2. *Atmospheric Chemistry and Physics Discussions*, *11*(8), 22893–22907. https://doi.org/10.5194/acpd-11-22893-2011

Côté, J., Gravel, S., Méthot, A., Patoine, A., Roch, M., & Staniforth, A. (1998). The operational CMC-MRB global environmental multiscale (GEM) model. Part I: Design considerations and formulation. *Monthly Weather Review*, *126*(6), 1373–1395. https://doi.org/10.1175/1520-0493(1998)126<1373:TOCMGE>2.0.CO;2

Dee, D. P., Uppala, S. M., Simmons, A. J., Berrisford, P., Poli, P., Kobayashi, S., et al. (2011). The ERA-Interim reanalysis: Configuration and performance of the data assimilation system. *Quarterly Journal of the Royal Meteorological Society*, *137*(656), 553–597. https://doi.org/10.1002/qj.828

Delage, Y. (1997). Parameterising sub-grid scale vertical transport in atmospheric models under statically stable conditions. *Boundary-Layer Meteorology*, *82*(1), 23–48. https://doi.org/10.1023/a:1000132524077

Delage, Y., & Girard, C. (1992). Stability functions correct at the free convection limit and consistent for for both the surface and Ekman layers. *Boundary-Layer Meteorology*, *58*(1), 19–31. https://doi.org/10.1007/bf00120749

Deser, C., Tomas, R., Alexander, M., & Lawrence, D. (2010). The seasonal atmospheric response to projected Arctic sea ice loss in the late twenty-first century. *Journal of Climate*, *23*(2), 333–351. https://doi.org/10.1175/2009JCLI3053.1

Devasthale, A., Willén, U., Karlsson, K. G., & Jones, C. G. (2010). Quantifying the clear-sky temperature inversion frequency and strength over the Arctic Ocean during summer and winter seasons from AIRS profiles. *Atmospheric Chemistry and Physics*, *10*(12), 5565–5572. https://doi.org/10.5194/acp-10-5565-2010

Durre, I., Vose, R. S., & Wuertz, D. B. (2006). Overview of the integrated global radiosonde archive. *Journal of Climate*, *19*(1), 53–68. https://doi.org/10.1175/JCLI3594.1

Fernando, H. J. S., & Weil, J. C. (2010). Whither the stable boundary layer? *Bulletin of the American Meteorological Society*, *91*(11), 1475–1484. https://doi.org/10.1175/2010BAMS2770.1

Fochesatto, G. J. (2015). Methodology for determining multilayered temperature inversions. *Atmospheric Measurement Techniques*, *8*(5), 2051–2060. https://doi.org/10.5194/amt-8-2051-2015

Gilson, G., Jiskoot, H., Cassano, J., Gultepe, I., & James, T. (2018). The Thermodynamic Structure of Arctic Coastal Fog Occurring During the Melt Season over East Greenland. *Boundary-Layer Meteorology*, *168*. https://doi.org/10.1007/s10546-018-0357-3

Gultepe, I., Isaac, G. A., Williams, A., Marcotte, D., & Strawbridge, K. B. (2003). Turbulent heat fluxes over leads and polynyas, and their effects on arctic clouds during FIRE.ACE: Aircraft observations for April 1998. *Atmosphere - Ocean*, *41*(1), 15–34. https://doi.org/10.3137/ao.410102

Harris, I., Jones, P. D., Osborn, T. J., & Lister, D. H. (2014). Updated high-resolution grids of monthly climatic observations - the CRU TS3.10 Dataset. *International Journal of Climatology*, *34*(3), 623–642. https://doi.org/10.1002/joc.3711

Hearty, T. J., Savtchenko, A., Tian, B., Fetzer, E., Yung, Y. L., Theobald, M., et al. (2014). Estimating sampling biases and measurement uncertainties of AIRS/AMSU-A temperature and water vapor observations using MERRA reanalysis. *Journal of Geophysical Research*, *119*(6), 2725–2741. https://doi.org/10.1002/2013JD021205

Holtslag, A. A. M., Svensson, G., Baas, P., Basu, S., Beare, B., Beljaars, A. C. M., et al. (2013). Stable atmospheric boundary layers and diurnal cycles: Challenges for weather and climate models. *Bulletin of the American Meteorological Society*, *94*(11), 1691–

1706. https://doi.org/10.1175/BAMS-D-11-00187.1

Hwang, Y. T., Frierson, D. M. W., & Kay, J. E. (2011). Coupling between Arctic feedbacks and changes in poleward energy transport. *Geophysical Research Letters*, *38*(17), n/a-n/a. https://doi.org/10.1029/2011GL048546

IPCC. (2013). *Climate Change 2013 - The Physical Science Basis*. *Climate Change 2013 - The Physical Science Basis*. https://doi.org/10.1017/cbo9781107415324

Kahl, J. D. (1990). Characteristics of the low-level temperature inversion along the Alaskan Arctic coast. *International Journal of Climatology*, *10*(5), 537–548. https://doi.org/10.1002/joc.3370100509

Kain, J. S., & Fritsch, J. M. (1990). A one-dimensional entraining/detraining plume model and its application in convective parameterization. *Journal of the Atmospheric Sciences*, *47*(23), 2784–2802. https://doi.org/10.1175/1520-0469(1990)047<2784:AODEPM>2.0.CO;2

Kim, K.-Y., Kim, J.-Y., Kim, J., Yeo, S., Na, H., Hamlington, B. D., & Leben, R. R. (2019). Vertical Feedback Mechanism of Winter Arctic Amplification and Sea Ice Loss. *Scientific Reports*, *9*(1), 1184. https://doi.org/10.1038/s41598-018-38109-x

Koenigk, T., Brodeau, L., Graversen, R. G., Karlsson, J., Svensson, G., Tjernström, M., et al. (2013). Arctic climate change in 21st century CMIP5 simulations with EC-Earth. *Climate Dynamics*, *40*(11–12), 2719–2743. https://doi.org/10.1007/s00382-012-1505-y

Koenigk, T., Key, J., & Vihma, T. (2020). Climate Change in the Arctic (pp. 673–705). Springer, Cham. https://doi.org/10.1007/978-3-030-33566-3_11

Kuo, H. L. (1965). On Formation and Intensification of Tropical Cyclones Through Latent Heat Release by Cumulus Convection. *Journal of the Atmospheric Sciences*, *22*(1), 40–63. https://doi.org/10.1175/1520-0469(1965)022<0040:ofaiot>2.0.co;2

Lawrence, D. M., Slater, A. G., Tomas, R. A., Holland, M. M., & Deser, C. (2008). Accelerated Arctic land warming and permafrost degradation during rapid sea ice loss. *Geophysical Research Letters*, *35*(11), L11506. https://doi.org/10.1029/2008GL033985

Li, J., & Barker, H. W. (2005). A radiation algorithm with correlated-k distribution. Part I: Local thermal equilibrium. *Journal of the Atmospheric Sciences*, *62*(2), 286–309. https://doi.org/10.1175/JAS-3396.1

Lindsay, R., Wensnahan, M., Schweiger, A., & Zhang, J. (2014). Evaluation of seven different atmospheric reanalysis products in the arctic. *Journal of Climate*, *27*(7), 2588–2606. https://doi.org/10.1175/JCLI-D-13-00014.1

Liu, Y., Key, J. R., Liu, Z., Wang, X., & Vavrus, S. J. (2012). A cloudier Arctic expected with diminishing sea ice. *Geophysical Research Letters*, *39*(5), n/a-n/a. https://doi.org/10.1029/2012GL051251

Liu, Y., Key, J. R., Schweiger, A., & Francis, J. (2006). Characteristics of satellite-derived clear-sky atmospheric temperature inversion strength in the Arctic, 1980-96. *Journal of Climate*, *19*(19), 4902–4913. https://doi.org/10.1175/JCLI3915.1

Mahrt, L. (1998). Stratified atmospheric boundary layers and breakdown of models. *Theoretical and Computational Fluid Dynamics*, *11*(3–4), 263–279. https://doi.org/10.1007/s001620050093

McFarlane, N. A. (1987). The Effect of Orographically Excited Gravity Wave Drag on the General Circulation of the Lower Stratosphere and Troposphere. *Journal of the Atmospheric Sciences*, *44*(14), 1775–1800. https://doi.org/10.1175/1520-0469(1987)044<1775:teooeg>2.0.co;2

Medeiros, B., Deser, C., Tomas, R. A., & Kay, J. E. (2011). Arctic inversion strength in climate models. *Journal of Climate*, *24*(17), 4733–4740.

https://doi.org/10.1175/2011JCLI3968.1

Mironov, D., Rontu, L., Kourzeneva, E., & Terzhevik, A. (2010). Towards improved representation of lakes in numerical weather prediction and climate models: Introduction to the special issue of Boreal Environment Research. *Boreal Environment Research*, *15*(97–99).

Morrison, A. L., Kay, J. E., Frey, W. R., Chepfer, H., & Guzman, R. (2019). Cloud Response to Arctic Sea Ice Loss and Implications for Future Feedback in the CESM1 Climate Model. *Journal of Geophysical Research: Atmospheres*, *124*(2), 1003–1020. https://doi.org/10.1029/2018JD029142

Palo, T., Vihma, T., Jaagus, J., & Jakobson, E. (2017). Observations of temperature inversions over central Arctic sea ice in summer. *Quarterly Journal of the Royal Meteorological Society*, *143*(708), 2741–2754. https://doi.org/10.1002/qj.3123

Pavelsky, T. M., Boé, J., Hall, A., & Fetzer, E. J. (2011). Atmospheric inversion strength over polar oceans in winter regulated by sea ice. *Climate Dynamics*, *36*(5–6), 945–955. https://doi.org/10.1007/s00382-010-0756-8

Riahi, K., Rao, S., Krey, V., Cho, C., Chirkov, V., Fischer, G., et al. (2011). RCP 8.5-A scenario of comparatively high greenhouse gas emissions. *Climatic Change*, *109*(1), 33–57. https://doi.org/10.1007/s10584-011-0149-y

Screen, J. A., & Simmonds, I. (2010a). Increasing fall-winter energy loss from the Arctic Ocean and its role in Arctic temperature amplification. *Geophysical Research Letters*, *37*(16), n/a-n/a. https://doi.org/10.1029/2010GL044136

Screen, J. A., & Simmonds, I. (2010b). The central role of diminishing sea ice in recent Arctic temperature amplification. *Nature*, *464*(7293), 1334–1337. https://doi.org/10.1038/nature09051

Šeparović, L., Alexandru, A., Laprise, R., Martynov, A., Sushama, L., Winger, K., et al. (2013). Present climate and climate change over North America as simulated by the fifth-generation Canadian regional climate model. *Climate Dynamics*, *41*(11–12), 3167–3201. https://doi.org/10.1007/s00382-013-1737-5

Serreze, M. C., Barrett, A. P., Stroeve, J. C., Kindig, D. N., & Holland, M. M. (2009). The emergence of surface-based Arctic amplification. *Cryosphere*, *3*(1), 11–19. https://doi.org/10.5194/tc-3-11-2009

Serreze, Mark C., & Barry, R. G. (2006). The Arctic climate system. *Choice Reviews Online*, *44*(01), 44-0373-44–0373. https://doi.org/10.5860/choice.44-0373

Sundqvist, H., Berge, E., & Kristjansson, J. E. (1989). Condensation and cloud parameterization studies with a mesoscale numerical weather prediction model. *Monthly Weather Review*, *117*(8), 1641–1657. https://doi.org/10.1175/1520-0493(1989)117<1641:CACPSW>2.0.CO;2

Teufel, B., & Sushama, L. (2019). Abrupt changes across the Arctic permafrost region endanger northern development. *Nature Climate Change*. Nature Publishing Group. https://doi.org/10.1038/s41558-019-0614-6

Tian, B., Fetzer, E. J., Kahn, B. H., Teixeira, J., Manning, E., & Hearty, T. (2013). Evaluating CMIP5 models using AIRS tropospheric air temperature and specific humidity climatology. *Journal of Geophysical Research Atmospheres*, *118*(1), 114–134. https://doi.org/10.1029/2012JD018607

Tjernström, M., Shupe, M. D., Brooks, I. M., Achtert, P., Prytherch, J., & Sedlar, J. (2019). Arctic summer airmass transformation, surface inversions, and the surface energy budget. *Journal of Climate*, *32*(3), 769–789. https://doi.org/10.1175/JCLI-D-18-0216.1

Van de Wiel, B. J. H., Vignon, E., Baas, P., van Hooijdonk, I. G. S., van der Linden, S. J. A., van Hooft, J. A., et al. (2017). Regime transitions in near-surface temperature inversions: A conceptual model. *Journal of the Atmospheric Sciences*, *74*(4), 1057–1073. https://doi.org/10.1175/JAS-D-16-0180.1

van Vuuren, D. P., Edmonds, J., Kainuma, M., Riahi, K., Thomson, A., Hibbard, K., et al. (2011). The representative concentration pathways: An overview. *Climatic Change*, *109*(1), 5–31. https://doi.org/10.1007/s10584-011-0148-z

Vavrus, S. J., Holland, M. M., Jahn, A., Bailey, D. A., & Blazey, B. A. (2012). Twenty-first-century arctic climate change in CCSM4. *Journal of Climate*, *25*(8), 2696–2710. https://doi.org/10.1175/JCLI-D-11-00220.1

Verseghy, D. (2009). CLASS - The Canadian Land Surface Scheme (Version 3.4), Technical Documentation (Version 1.1). *Climate Research Division, Science and Technology Branch, Downsview, Ontario, Canada*, (January), 180.

Verseghy, D. L., McFarlane, N. A., & Lazare, M. (1993). CLASS - A Canadian land surface scheme for GCMS, II. Vegetation model and coupled runs. *International Journal of Climatology*, *13*(4), 347–370. https://doi.org/10.1002/joc.3370130402

Verseghy, Diana L. (1991). CLASS - A Canadian land surface scheme for GCMS. I. Soil model. *International Journal of Climatology*, *11*(2), 111–133. https://doi.org/10.1002/joc.3370110202

Wang, D., Guo, J., Chen, A., Bian, L., Ding, M., Liu, L., et al. (2020). Temperature Inversion and Clouds Over the Arctic Ocean Observed by the 5th Chinese National Arctic Research Expedition. *Journal of Geophysical Research: Atmospheres*, *125*(13), e2019JD032136. https://doi.org/10.1029/2019JD032136

Wang, X. ;, Liu, J. ;, Liu, H. ;, Bhatt, S., Wang, M., Wang, X., et al. (2022). Characteristics of Arctic Summer Inversion and Its Correlation with Extreme Sea Ice Anomalies.

Atmosphere 2022, Vol. 13, Page 316, *13*(2), 316. https://doi.org/10.3390/ATMOS13020316

Wetzel, C., & Brümmer, B. (2011). An Arctic inversion climatology based on the European Centre Reanalysis ERA-40. *Meteorologische Zeitschrift*, *20*(6), 589–600. https://doi.org/10.1127/0941-2948/2011/0295

Yeh, K. S., Côté, J., Gravel, S., Méthot, A., Patoine, A., Roch, M., & Staniforth, A. (2002). The CMC-MRB Global Environmental Multiscale (GEM) model. Part III: Nonhydrostatic formulation. *Monthly Weather Review*, *130*(2), 339–356. https://doi.org/10.1175/1520-0493(2002)130<0339:TCMGEM>2.0.CO;2

Zadra, A., Roch, M., Laroche, S., & Charron, M. (2003). The subgrid-scale orographic blocking parametrization of the GEM Model. *Atmosphere-Ocean*, *41*(2), 155–170. https://doi.org/10.3137/ao.410204

Zhang, Lei, Li, J., Ding, M., Guo, J., Bian, L., Sun, Q., et al. (2021). Characteristics of low-level temperature inversions over the Arctic Ocean during the CHINARE 2018 campaign in summer. *Atmospheric Environment*, *253*, 118333. https://doi.org/10.1016/j.atmosenv.2021.118333

Zhang, Lin, Ding, M., Dou, T., Huang, Y., Lv, J., & Xiao, C. (2021). The shallowing surface temperature inversions in the arctic. *Journal of Climate*, *34*(10), 4159–4168. https://doi.org/10.1175/JCLI-D-20-0621.1

Zhang, Y., & Seidel, D. J. (2011). Challenges in estimating trends in Arctic surface-based inversions from radiosonde data. *Geophysical Research Letters*, *38*(17), n/a-n/a. https://doi.org/10.1029/2011GL048728

Zhang, Y., Seidel, D. J., Golaz, J. C., Deser, C., & Tomas, R. A. (2011). Climatological characteristics of Arctic and Antarctic surface-based inversions. *Journal of Climate*, *24*(19), 5167–5186. https://doi.org/10.1175/2011JCLI4004.1

TABLES

Table 1: Subset of radiosonde values plus standard deviation for the temperature inversion strength (ΔT) and the temperature inversion frequency (FREQ), with corresponding values from the GEM-ERA simulation for summer and winter.

	DJF				JJA			
	Soundings		GEM-ERA		Soundings		GEM-ERA	
Location (lat, lon)	ΔT (°C)	FREQ (%)	ΔT (°C)	FREQ (%)	ΔT (°C)	FREQ (%)	ΔT (°C)	FREQ (%)
ZYRYANKA (65.7, 150.9)	11.8±6.6	87	7.5±5.2	60	1.8±1.5	13	2.6±2.0	19
SEJMCHAN (62.9, 152.4)	9.4±5.1	79	5.2±4.3	51	3.2±2.2	25	3.8±3.1	29
SODANKYLA (67.4, 26.6)	7.9±6.1	53	7.5±5.2	66	2.7±1.9	21	1.8±1.5	8
OSTROV DIKSON (73.5, -80.4)	6.3±3.7	78	5.9±3.9	59	3.1±2.4	32	3.2±2.2	41
ARHANGEL'SK (64.6, 40.5)	5.1±3.8	44	5.2±3.8	42	2.6±1.8	23	1.4±1.2	8
BAKER LAKE (64.3, -96.1)	7.8±4.2	90	8.1±5.5	75	2.8±2.2	20	2.1±1.8	20
INUVIK (68.3, -133.5)	7.4±4.9	80	10.7±7.6	74	2.3±2	25	2.3±1.8	22
ALERT (82.5, -62.3)	5.8±4.0	82	9.5±5.9	84	3.0±2.1	43	4.5±3.1	52

FIGURES

Figures should include full captions. Appendix figures should be included here following any main manuscript figures (if any).

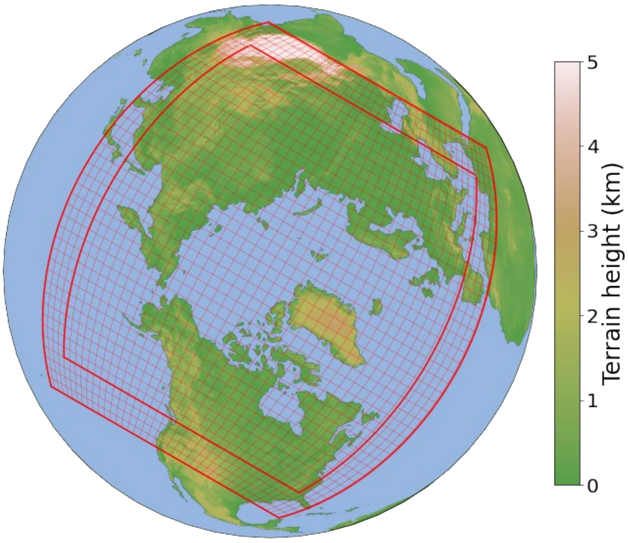

Fig. 1 **The Pan-Arctic experimental domain, with every fifth grid point shown. The inner bold line separates the blending and free zones. The topography is shown in color.**

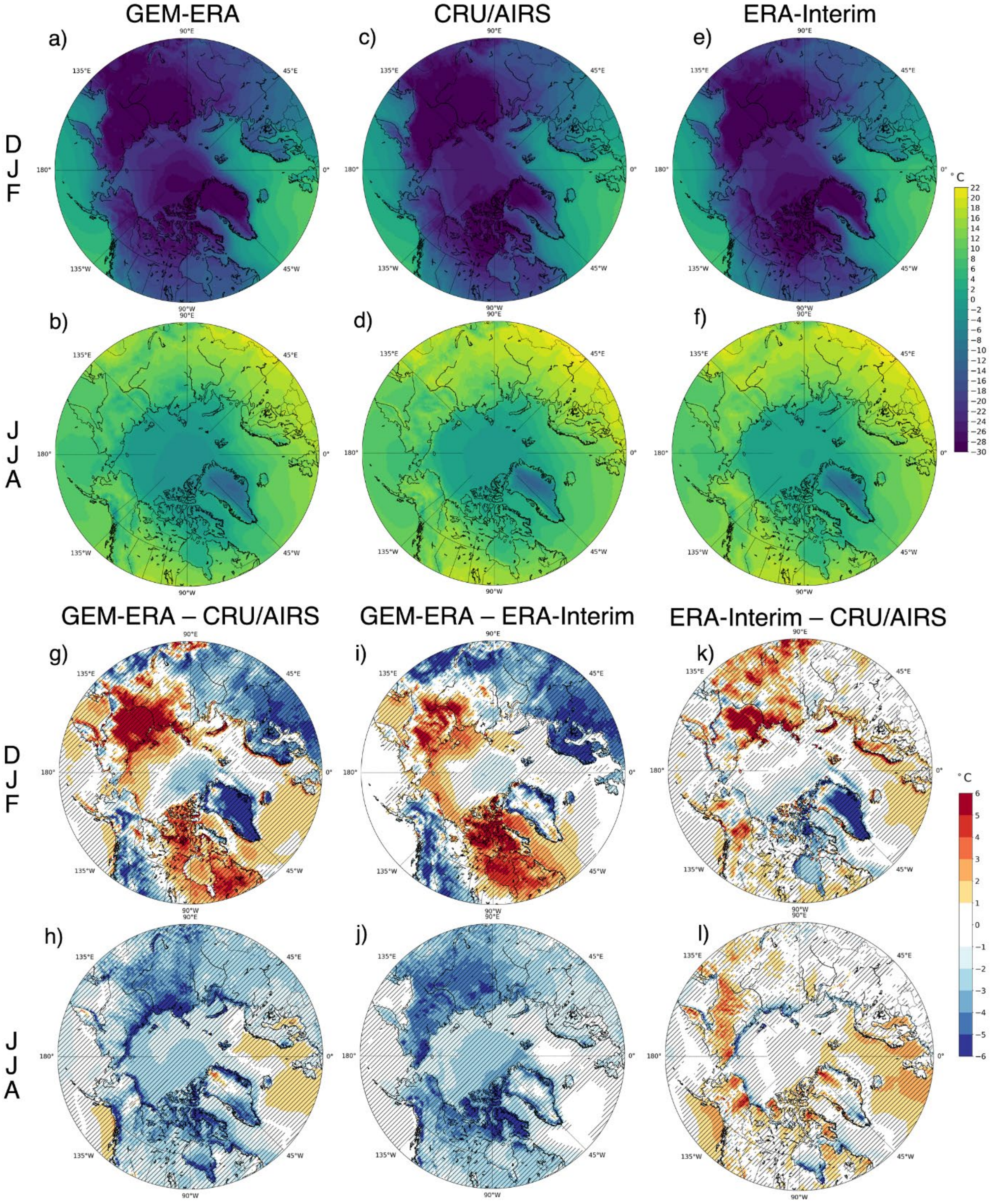

Fig. 2 Spatial plots showing 2m temperatures for the 2003-2015 period for: GEM-ERA simulated climatological winter (a) and summer (b); CRU (land) and AIRS (ocean) winter (c) and summer (d); ERA-Interim winter (e) and summer (f). Differences between GEM-ERA and CRU/AIRS 2m temperatures for winter (g) and summer (h), and

differences between GEM-ERA and ERA-Interim for winter (i) and summer (j). Hatched regions show where projected changes are statistically significant with the two-sample t-test at the 5% significance level.

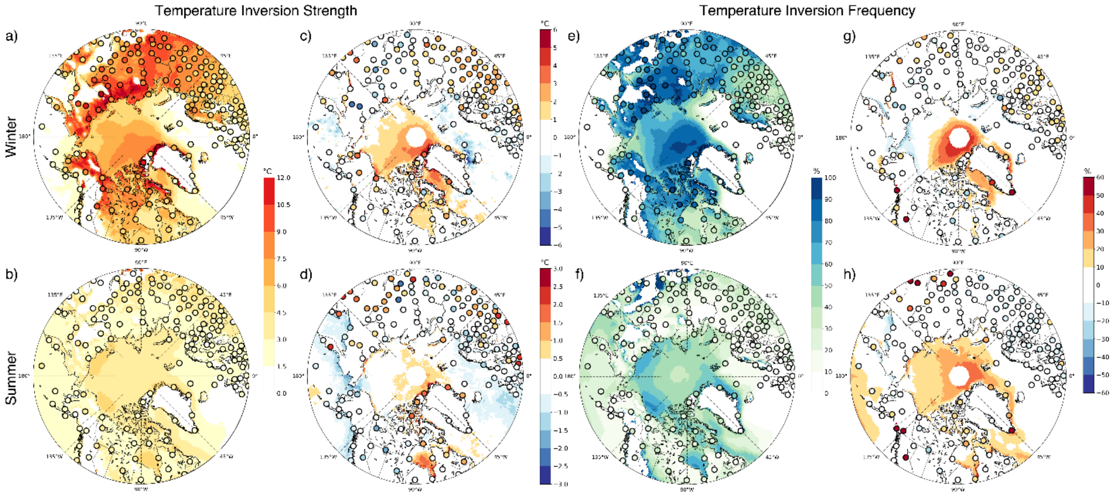

Fig. 3 **GEM-ERA simulated winter (a) and summer (b) temperature inversion strength. Winter (c) and summer (d) differences between GEM-ERA and ARIS (ocean) and atmospheric soundings (circles over land) for the temperature inversion strength. e)-(h): same as (a)-(d) for the temperature inversion frequency.**

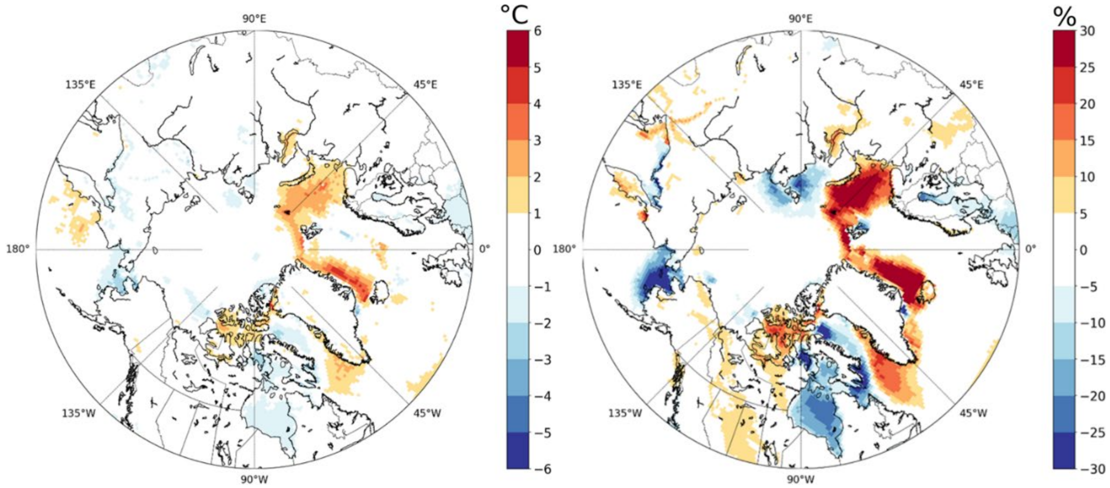

Fig. 4 Difference between GEM-ERA and GEM-CAN simulations in DJF for temperature inversion strength (left column) and inversion frequency (right column for the 1980-2005 period

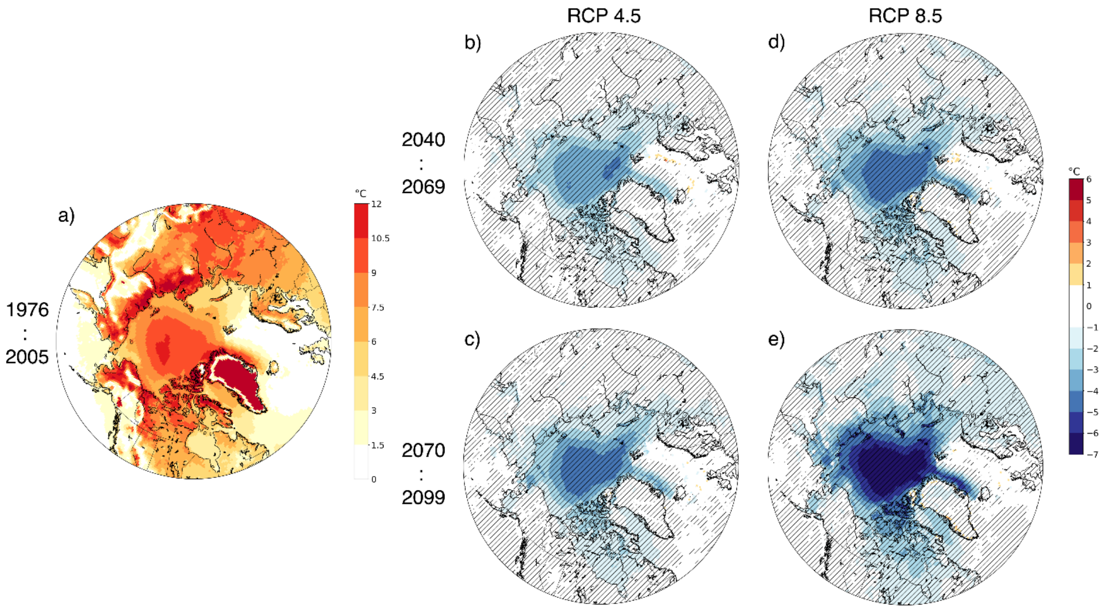

Fig. 5 **GEM-CAN simulated temperature inversion strength for DJF (a) and RCP 4.5 projected changes to DJF temperature inversion strength for the 2040–2069 (b) and 2070–2099 (c) future periods with respect to the current 1976–2005 period. (d)-(e): same as (b) and (c) but for RCP 8.5. Hatched regions show where projected changes are statistically significant with the two-sample t-test at the 5% significance level.**

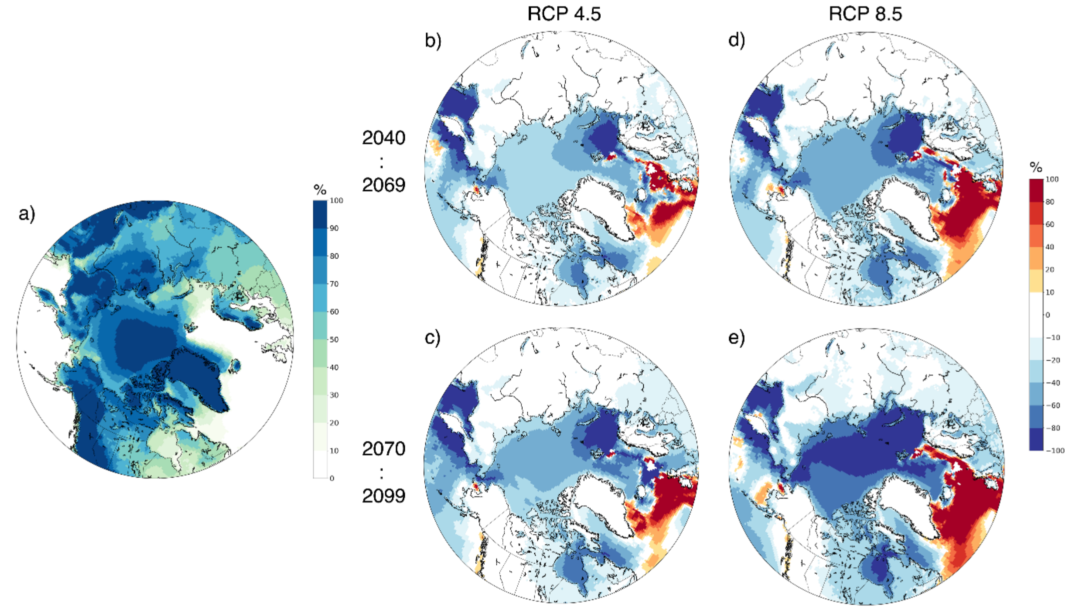

Fig. 6 **GEM-CAN simulated temperature inversion frequency for DJF (a) and RCP 4.5 projected changes to DJF temperature inversion strength for the 2040–2069 (b) and 2070–2099 (c) future periods with respect to the current 1976–2005 period. (d)-(e): same as (b) and (c) but for RCP 8.5.**

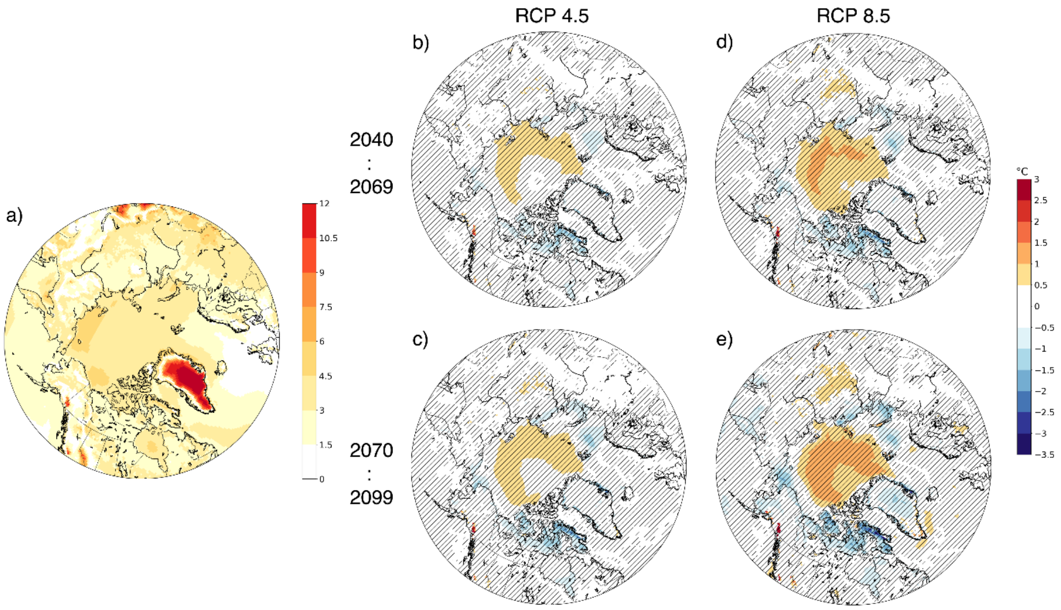

Fig. 7 **GEM-CAN simulated temperature inversion strength for JJA (a) and RCP 4.5 projected changes to JJA temperature inversion strength for the 2040–2069 (b) and 2070–2099 (c) future periods with respect to the current 1976–2005 period. (d)-(e): same as (b) and (c) but for RCP 8.5. Hatched regions show where projected changes are statistically significant with the two-sample t-test at the 5% significance level.**

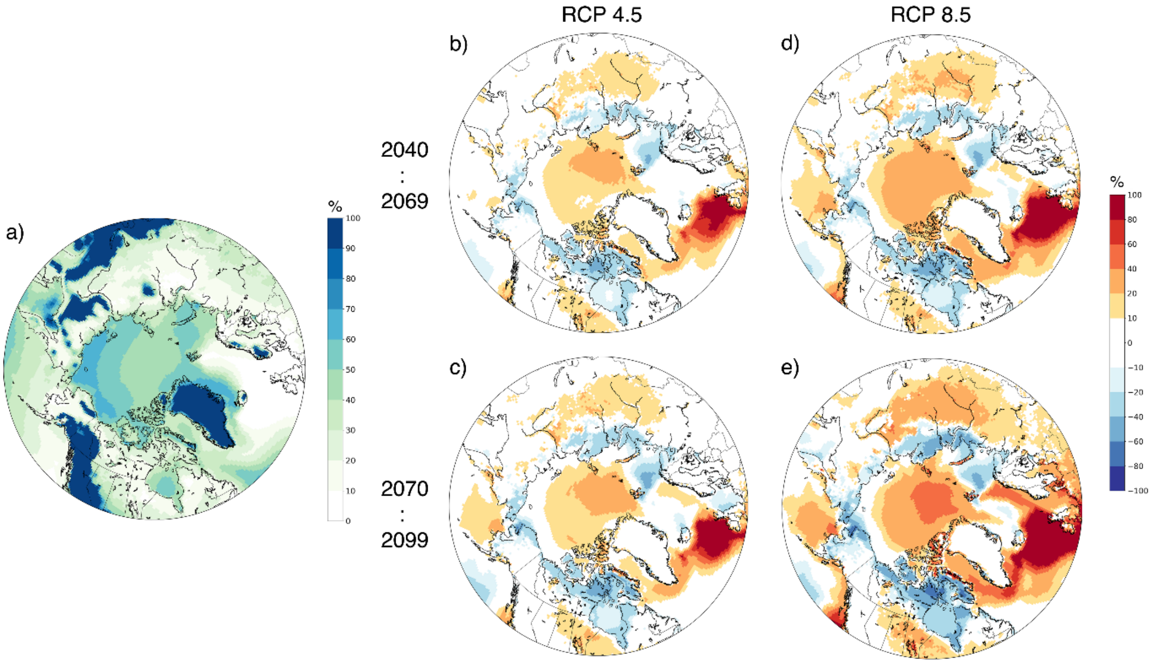

Fig. 8 **GEM-CAN simulated temperature inversion frequency for JJA (a) and RCP 4.5 projected changes to JJA temperature inversion frequency for the 2040–2069 (b) and 2070–2099 (c) future periods with respect to the current 1976–2005 period. (d)-(e): same as (b) and (c) but for RCP 8.5.**

Climatology of Arctic temperature inversions in current and future climates

C. J. Ruman,[a] A. H. Monahan,[b] L. Sushama,[a]

[a] *Department of Civil Engineering and Applied Mechanics, McGill University, Montréal, QC, Canada*

[b] *School of Earth and Ocean Sciences, University of Victoria, Victoria, BC, Canada*

Corresponding author: Caio Jorge Ruman, caio.ruman@mail.mcgill.ca

Supplementary Figures

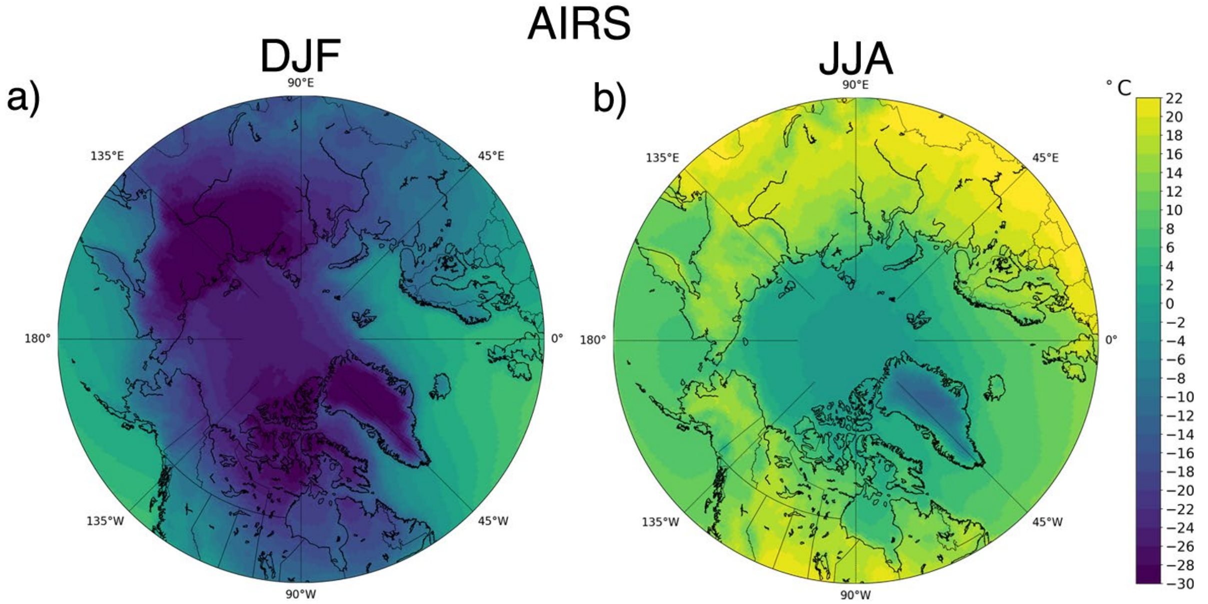

Fig. S1: **Spatial plots showing 2m temperatures for the 2003-2015 period for the AIRS dataset for the winter (a) and summer (b) months.**

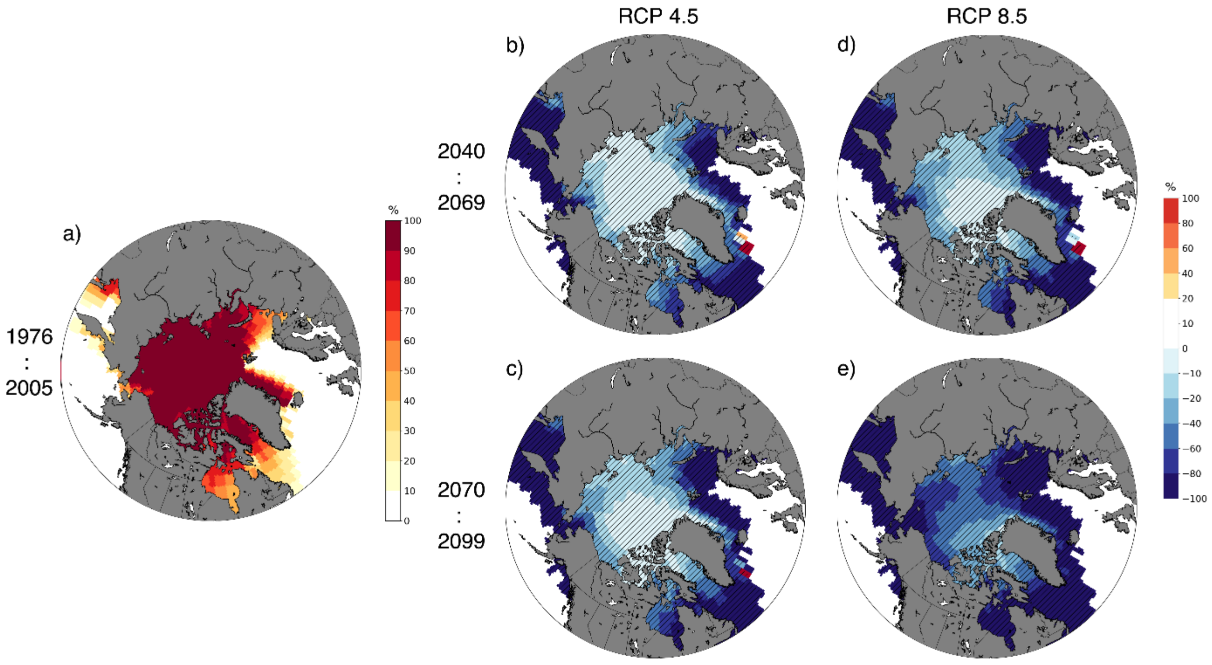

Fig. S2: **GEM-CAN simulated sea-ice for DJF (a) and RCP 4.5 projected changes to DJF sea-ice for the 2040–2069 (b) and 2070–2099 (c) future periods with respect to the current 1976–2005 period. (d)-(e): same as (b) and (c) but for RCP 8.5.**

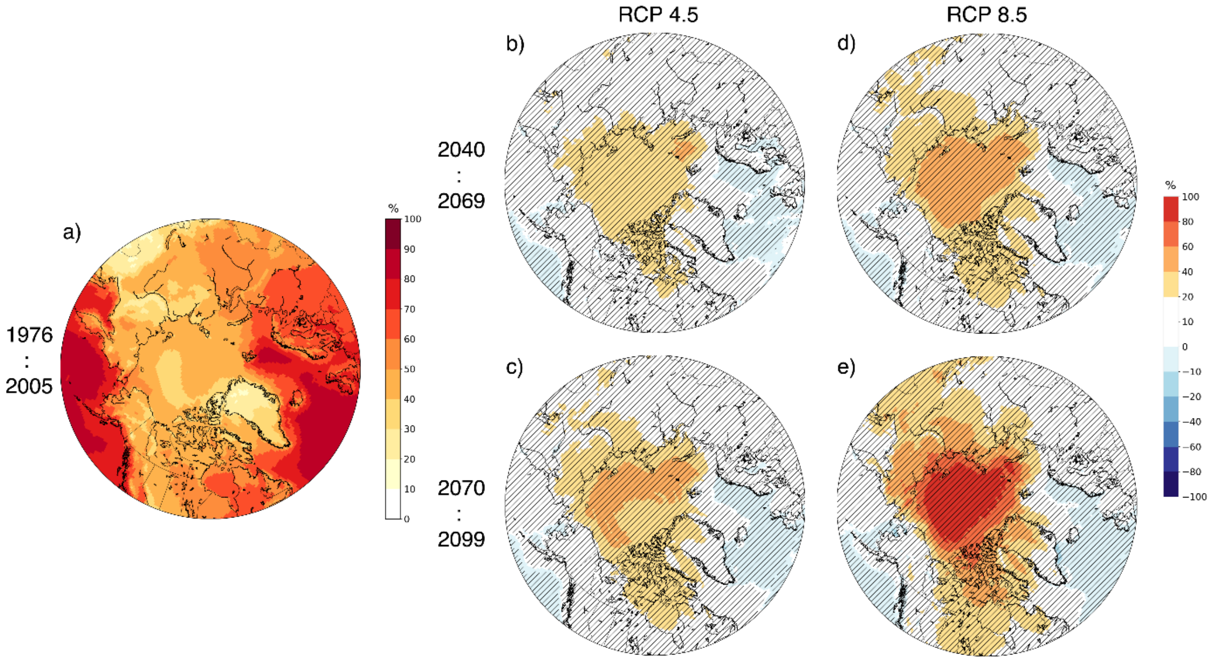

Fig. S3: **GEM-CAN simulated total cloud cover for DJF (a) and RCP 4.5 projected changes to DJF total cloud for the 2040–2069 (b) and 2070–2099 (c) future periods with respect to the current 1976–2005 period. (d)-(e): same as (b) and (c) but for RCP 8.5.**